Available online at www.sciencedirect.com
SCIENCE DIRECT®
Journal of Nuclear Materials 342 (2005) 119–124
journal of nuclear materials
www.elsevier.com/locate/jnucmat

Thermal conductivity of near-stoichiometric $(U,Er)O_2$ solid solutions

Si-Hyung Kim [a,b,*], Yeon-Gu Kim [a], Han-Soo Kim [a], Sang-Ho Na [a], Young-Woo Lee [a], Dong-Soo Suhr [b]

[a] *Korea Atomic Energy Research Institute, P.O. Box 105, Yusong, Daejon 305-600, South Korea*
[b] *Department of Materials Engineering, Chung-Nam National University, Daejon 305-764, South Korea*

Received 17 December 2004; accepted 24 March 2005

Abstract

Thermal diffusivities of UO_2 and UO_2 doped with 1, 3, 5, 7 and 10 mol % $ErO_{1.5}$ were measured in the range of 298–1673 K by a laser flash method and their thermal conductivities were calculated from the thermal diffusivity, the measured sample density and published specific heat capacity data. The temperature dependence of the thermal conductivity up to 1673 K in UO_2 and UO_2-doped with $ErO_{1.5}$ was found to be modeled well using the phonon conduction equation, $K = (A + BT)^{-1}$. The thermal conductivities of the UO_2 and $(U,Er)O_2$ solid solutions gradually decreased with the temperature. The thermal conductivity of the doped UO_2 decreased relative to UO_2 with an increase of $ErO_{1.5}$ content at low temperatures, while it was independent of the $ErO_{1.5}$ content at higher temperatures. The variation of parameters A and B as a function of $ErO_{1.5}$ content is found experimentally and it is found that the dependence of the thermal conductivity of $(U,Er)O_2$ on temperature up to 1673 K and on the $ErO_{1.5}$ content can be expressed as $K = \frac{K_{UO_2}}{1+K_{UO_2}(k_A y + k_B y T)}$.

1. Introduction

A burnable poison may be added to a reactor core in order to allow a larger initial fuel loading and to have a longer core operation life-time before refueling becomes necessary. Erbium is considered as a slow burnable poison suitable for use in a PWR reactor for a high burnup and/or extended cycle operation [1].

During the sintering of Er-doped UO_2 pellets at a high temperature, Er is known to form a solid solution with uranium dioxide, by substituting the uranium cations in the fluorite structure [2]. Therefore, the addition of Er to the UO_2 matrix influences the lattice structure and thermodynamic properties due to the differences in the charge and the size of the cations [3].

Thermal conductivity is one of the most important properties of nuclear reactor fuel pellets, as it directly influences the fuel operating temperatures, and the fuel operating temperature directly affects the fuel performance and behaviors such as fission gas release and swelling. A number of studies related to the effects of the addition of burnable poison such as $GdO_{1.5}$ to the thermal conductivity of UO_2 have been published

* Corresponding author. Address: Korea Atomic Energy Research Institute, P.O. Box 105, Yusong, Daejon 305-600, South Korea.
E-mail address: exodus@kaeri.re.kr (S.-H. Kim).

0022-3115/$ - see front matter © 2005 Elsevier B.V. All rights reserved.
doi:10.1016/j.jnucmat.2005.03.020

[4–11]. However, there is no report on the thermal conductivity for an Er-doped UO_2 pellet.

In this work, thermal conductivities of near-stoichiometric $(U_{1-y}Er_y)O_2$ solid solutions, $0 \leqslant y \leqslant 0.1$, were determined from room temperature to 1673 K.

2. Experimental

The starting materials were IDR-UO_2 purchased from BNFL (British Nuclear Fuels plc) and $ErO_{1.5}$ powder with a purity of 99.99% (Aldrich Chemical Company). The UO_2 powder was mixed with weighed amounts of $ErO_{1.5}$ powder, at concentrations of 1, 3, 5, 7, 9, 10 and 20 mol %, by a Turbula® mixer for 1 h and then successively milled by a dynamic ball mill for 1–6 h to prepare specimens of a similar density. UO_2-doped with 20 mol % $ErO_{1.5}$ was used only to measure the lattice parameter. Zinc stearate was used as a lubricant and admixed with the powder mixture. The milled oxide powders were compacted with a compaction pressure of 300 MPa and the green pellet specimens were sintered at 2023 K in flowing H_2 for 6 h. The densities of the samples were measured by the water immersion method.

The X-ray diffraction patterns were recorded in the range of $20° < 2\theta < 120°$ by using a monochromatic Cu-Kα radiation on an X-ray diffractometer (MXP 3A-HF, MacScience). The lattice parameters of the $(U_{1-y}Er_y)O_2$ solid solutions, $0 \leqslant y \leqslant 0.2$, were calculated from all the reflections by employing the least-squares method for the Nelson–Riley extrapolation and the theoretical density of each sample was evaluated from its lattice parameter.

In the temperature range from room temperature to 1673 K, the thermal conductivities were calculated from the heat capacity, the sample density and the thermal diffusivity measured by the laser flash method (Netzsch LFA-417). The measurements of the thermal diffusivity were carried out three times at every test temperature step in a vacuum at a pressure of less than 10^{-5} Pa. The average value of these three measurements was used and the experimental uncertainty associated with these measurements was within 5%.

For the thermal diffusivity measurements, samples were prepared in the shape of discs with an 8 mm diameter and 1 mm thickness. A pulse of laser was projected on to the front surface of the pellet and the temperature rise on the rear side of the pellet was recorded as a transient signal by using an infrared detector. The thermal diffusivity (α) was calculated from the following relationship:

$$\alpha = \frac{W}{\pi}\frac{L^2}{t_{1/2}}, \tag{1}$$

where $t_{1/2}$ is the time in seconds to one-half of the maximum temperature rise at the rear surface of the sample and L is the sample thickness in millimeter. W is a dimensionless parameter which is a function of the relative heat loss from the sample during the measurement. Table 1 shows the disc thickness, lattice parameter, bulk density and theoretical density of each sample.

3. Results and discussion

3.1. Lattice parameter

Une and Oguma [12] analyzed the oxygen to metal (O/M) ratio of $(U_{1-y}Gd_y)O_2$ solid solutions with $0.04 \leqslant y \leqslant 0.27$, sintered in H_2 at 1973 K. Their results showed that O/M ratios of all the solid solutions within the range of y specified above were in the range of 1.995–2.000 independent of the $GdO_{1.5}$ content and were averaged to 1.997, just below the stoichiometric composition.

According to Tagawa and Fujino [13], hypostoichiometric $U_{1-y}LaO_{2-x}$ has been reported to oxidize easily in air, even at room temperature, to a near-stoichiometric composition.

Fukushima et al. [14,15] measured the lattice parameter and O/M ratios of $(U_{1-y}Nd_y)O_2$, $(U_{1-y}Sm_y)O_2$, $(U_{1-y}Eu_y)O_2$ and $(U_{1-y}Y_y)O_2$ solid solutions, containing up to about 15 mol % of rare earth elements, sintered at 1973 K in an Ar–8% H_2 mixture for 3 h. Their results showed that the O/M ratio of all the samples were very close to 2.000, in the range of 1.995–2.003, depending on the rare earth or yttrium content.

Table 1
Sample characteristics of the UO_2 and $(U,Er)O_2$ pellets

$ErO_{1.5}$ content (mol %)	Thickness (mm)	Lattice parameter (nm)	Sintered density (g/cm^3)	Theoretical density (g/cm^3)	Relative density (%T.D.)
0	1.104	0.5470	10.66	10.96	97.3
1	0.996	0.5468	10.52	10.94	96.2
3	1.041	0.5465	10.40	10.90	95.4
5	1.058	0.5461	10.41	10.87	95.8
7	1.092	0.5455	10.40	10.85	95.8
10	1.094	0.5444	10.44	10.82	96.5
20	1.000	0.5419	10.39	10.68	97.3

Although the O/M ratio of the samples was not measured chemically in this study, the deviation from the stoichiometry is assumed to be very small up to 10 mol % $ErO_{1.5}$ based on the near stoichiometric behavior of other substitutional impurities as discussed above. Therefore, we will indicate the chemical formulae of the Er-doped UO_2 solid solutions as approximately $(U_{1-y}Er_y)O_2$. The thermal diffusivity was measured for UO_2 with up to 10 mol % $ErO_{1.5}$ in this study.

Fig. 1 shows the variation of the lattice parameter of the $(U_{1-y}R_y)O_2$ solid solutions as a function of the $RO_{1.5}$ content, where R indicates Er, Nd, Sm, Eu or Y. The lattice parameter of the $(U_{1-y}R_y)O_2$ linearly decreases as a function of the $RO_{1.5}$ content and follows Vegard's law, indicating the formation of a complete solid solution between the UO_2 and $RO_{1.5}$ phases. Among these solid solutions, the change in the lattice parameter of the $(U,Er)O_2$ was very similar to that of the $(U,Y)O_2$ solid solution. A regression was performed on the measured lattice parameters of $(U,Er)O_2$ to express the variation of the lattice parameters as a linear equation. It can be expressed as:

$$\text{Lattice parameter } (a,\text{nm}) = 0.5471 - 0.0264y \quad (0 \leqslant y \leqslant 0.2), \tag{2}$$

where y denotes the Er content.

According to Ohmichi et al. [16], the lattice parameter decreases linearly with an increase in the concentration of the rare earth elements, and the dependence of the lattice parameter (a) on y is calculated using the ionic radii of R^{3+} (rare earth), U^{4+}, U^{5+} and U^{6+}. The values of da/dy in $(U_{1-y}Er_y)O_2$, calculated by using Ohmichi's approach and by taking 0.1004 nm for the eight-coordination effective ionic radius of Er^{3+} [17], were −0.0273 and −0.0156 for the oxidation state of U^{5+} and U^{6+}, respectively. In our study, the experimentally determined value of da/dy is −0.0264 and therefore, it indicates that U^{5+} exists in preference to U^{6+} in $(U_{1-y}Er_y)O_2$ containing up to 20 mol % of $ErO_{1.5}$.

3.2. Thermal diffusivity

Fig. 2 shows the thermal diffusivities of the $(U,Er)O_2$ solid solutions as a function of the temperature. The data of all the samples were normalized to 95% of the theoretical density by using the following equation [5]:

$$\alpha_{95} = \frac{\alpha_M[(1-0.05\eta)(1-P)]}{[1-\eta P)(1-0.05)]}, \tag{3}$$

where α_M, η and P are, respectively, the measured thermal diffusivity, the experimentally determined fit parameter including its temperature dependence and the porosity of the sample. Here, for the value of η, which is a function of T, the following equation suggested by Brandt and Neuer [18] was used:

$$\eta = 2.6 - 5 \times 10^{-4}(T - 273.15), \tag{4}$$

where T is the temperature in Kelvin. The thermal diffusivities of UO_2 and $(U,Er)O_2$ gradually decreased with the test temperature as shown in Fig. 2. Fig. 2 also shows the dependence of the thermal diffusivity as a function of $ErO_{1.5}$ content. The thermal diffusivity of $(U,Er)O_2$ decreased with an increase of the $ErO_{1.5}$ content at low temperatures while it was independent of the $ErO_{1.5}$ content at higher temperatures, above approximately 1473 K. These phenomena were also observed by Yang et al. [10] and Hirai and Ishimoto [5]. According to Yang et al. [10], the thermal diffusivities of $UO_{2.14}$ and $(U_{1-y}Gd_y)O_{2.14}$ with $y = 0.09$ and 0.17, were nearly the same above 1473 K. In the case of Hirai and Ishimoto [5], they measured the thermal diffusivity of $(U_{1-y}Gd_y)O_2$ with $y = 0.04$, 0.07, 0.1, 0.15, and the aforementioned trend was observed above 1700 K. However, Fukushima et al. [4,14,15] found that the

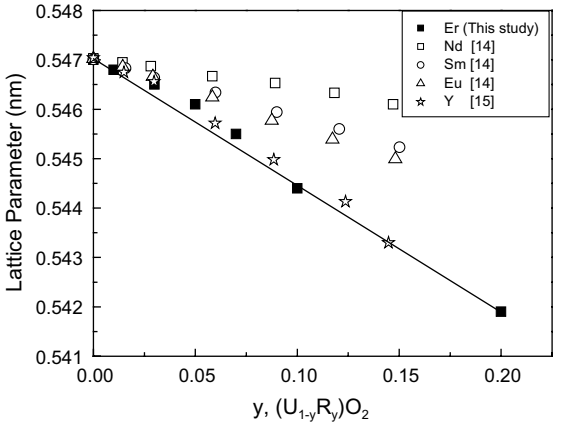

Fig. 1. Lattice parameters of the $(U_{1-y}R_y)O_2$ solid solutions as a function of the $RO_{1.5}$ content.

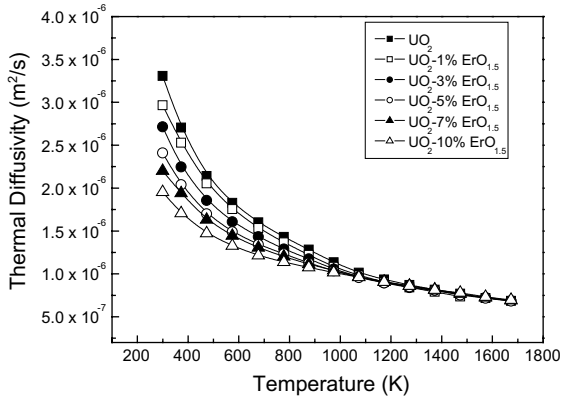

Fig. 2. Variation of the thermal diffusivity of the $(U,Er)O_2$ solid solutions with different $ErO_{1.5}$ content as a function of the temperature.

thermal diffusivity curves of the UO_2 and $(U,R)O_2$ solid solutions, where R is Gd, Nd, Sm, Eu or Y, exhibited a dependence on R up to 2000 K.

3.3. Thermal conductivity

The thermal conductivity (K) was calculated from the measured thermal diffusivity (α), specific heat capacity (C) and density (ρ) using the following relationship:

$$K = \alpha C \rho. \tag{5}$$

The heat capacities of the $(U_{1-y}Er_y)O_2$ solid solutions are not available in any literature. Generally, the unknown heat capacity values of solid solutions are estimated from those of individual component materials using the following expression (Neumann–Kopp equation):

$$C = \sum_i X_i C_i, \tag{6}$$

where X_i and C_i are the mole fraction and the heat capacity of the component i of the solid solution, respectively. The specific heat capacity of unirradiated UO_2 is available from the International Nuclear Safety Center (INSC) database of Argonne National Laboratory on the World-Wide Web [19] and that of $ErO_{1.5}$ is taken from the literature [20]. The density of $(U,Er)O_2$ at the test temperature is calculated from the value measured at room temperature by using the thermal expansion data of UO_2 [19].

The thermal conductivity normalized to 95% TD using Eq. (3) as a function of the temperature is shown in Fig. 3. The thermal conductivities of UO_2 and $(U,Er)O_2$ decrease with the temperature and that of UO_2 is in good agreement with that reported in the literature [19], for the entire temperature range of this study. As the temperature increases, the phonon–phonon scattering increases and thus the phonon mean free path decreases, resulting in a decrease in the thermal conductivity. Like the results of the thermal diffusivity, the thermal conductivities of $(U,Er)O_2$ decreased with an increase of the $ErO_{1.5}$ content at low temperatures and their thermal conductivities are nearly the same above 1473 K.

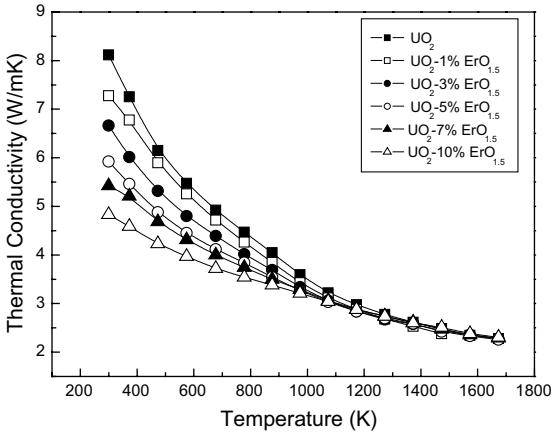

Fig. 3. Variation of the thermal conductivity of the $(U,Er)O_2$ solid solutions with different $ErO_{1.5}$ content as a function of the temperature.

In general, phonon–phonon scattering and phonon–impurity scattering are the dominant mechanisms on the thermal conductivity in a non-conductive solid (ceramics). Klemens [21] has proposed a heat conduction model in materials where phonon–phonon (Umklapp) scattering and phonon–impurity scattering occur simultaneously. If the additive resistance approximation is assumed, the thermal conductivity of insulating solids is given by the following equation [21,22]:

$$K = (A + BT)^{-1}, \tag{7}$$

where K is the thermal conductivity, T is the temperature in Kelvin and A and B are constants that are related to the phonon–impurity and phonon–phonon (Umklapp) scattering processes, respectively. Eq. (7) reflects the fact that, above the Debye temperature, phonon–phonon scattering is proportional to the temperature, whereas phonon–impurity scattering can normally be assumed to be independent of the temperature. Values of A and B can be determined by a least squares fit of Eq. (7) to the thermal conductivity data. Eq. (7) does not express very well the quantitative relation between the thermal conductivity and the content of impurities in the sample, but, as shown below, Eq. (7) models the observed temperature dependence well.

Table 2 shows the values of A and B of $(U,Er)O_2$ determined by fitting the thermal conductivity data to Eq. (7). The values of A increase gradually with an increasing $ErO_{1.5}$ content, while those of B decrease slightly. The fact that the thermal conductivity is independent of $ErO_{1.5}$ content at high temperatures indicates that phonon–phonon scattering dominates at a high temperatures in $(U,Er)O_2$ solid solutions and phonon–impurity scattering dominates at low temperatures.

Taking the inverse of Eq. (7), the thermal resistivity R can be expressed as

$$R = \frac{1}{K} = A + BT = R_L + R_P, \tag{8}$$

Table 2
Measured values of A and B in Eq. (7) for the $(U,Er)O_2$ solid solutions

$ErO_{1.5}$ content (mol %)	A (mK/W)	B (m/W)
0	0.05253	0.00023
1	0.06472	0.00023
3	0.08400	0.00022
5	0.10749	0.00020
7	0.12559	0.00019
10	0.15811	0.00016

where R_L and R_P corresponds to A and BT in Eq. (8), respectively. In addition, in the case of a solid solution, the lattice defect thermal resistivity (R_L) can be generally expressed by the following equation:

$$R_L = A(0) + \Delta A(\mathrm{Er}), \tag{9}$$

where $A(0)$ is the lattice defect thermal resistivity caused by defects such as the impurities included in the sample and $\Delta A(\mathrm{Er})$ implies an additional defect thermal resistivity due to the dissolution of Er. Assuming $A(0)$ to be constant for all the samples, the value corresponds to the A of UO_2 expressed in Table 2. The relationship between $\Delta A(\mathrm{Er})$ and the $ErO_{1.5}$ content is shown in Fig. 4, which shows that $\Delta A(\mathrm{Er})$ is proportional to the $ErO_{1.5}$ content.

Since the measured values of B for $(U,Er)O_2$ are slightly decreased as a function of the $ErO_{1.5}$ content as shown in Table 2, the effect of an additional intrinsic thermal resistivity (R_P) should also be considered by the following equation:

$$R_P = B(0)T + \Delta B(\mathrm{Er})T, \tag{10}$$

where $B(0)$ is the intrinsic thermal resistivity which corresponds to the B value of UO_2 in Table 2 and $\Delta B(\mathrm{Er})$ is the additional intrinsic thermal resistivity caused by a dissolution of Er. The relationship between $\Delta B(\mathrm{Er})$ and the $ErO_{1.5}$ content is shown in Fig. 5 and the slope was obtained by a linear fitting.

Substituting Eqs. (9) and (10) into Eq. (8), the following expression for the thermal conductivity of $(U,Er)O_2$ can be obtained:

$$K = \frac{1}{R_L + R_P} = \frac{1}{A(0) + \Delta A(\mathrm{Er}) + B(0)T + \Delta B(\mathrm{Er})T}. \tag{11}$$

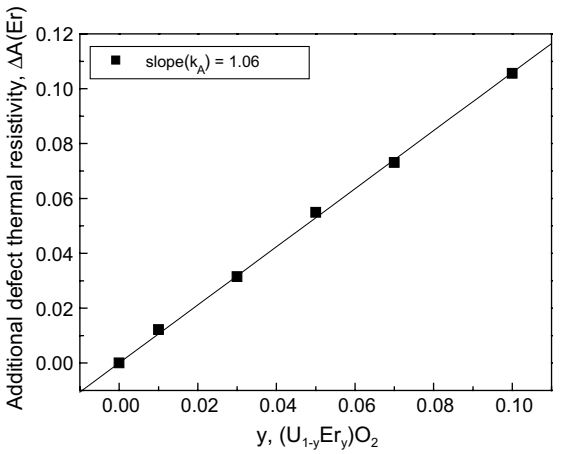

Fig. 4. Relationship between $\Delta A(\mathrm{Er})$ and the $y(ErO_{1.5})$ content in the $(U,Er)O_2$ solid solution.

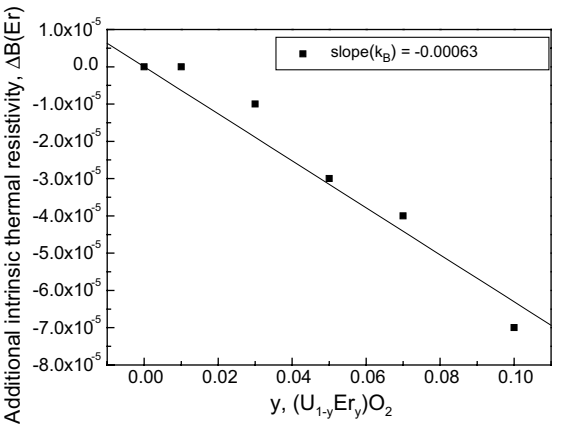

Fig. 5. Relationship between $\Delta B(\mathrm{Er})$ and the $y(ErO_{1.5})$ content in the $(U,Er)O_2$ solid solution.

The thermal conductivity of UO_2, K_{UO_2}, is given by

$$K_{UO_2} = \frac{1}{A(0) + B(0)T}. \tag{12}$$

Therefore, Eq. (11) becomes

$$K = \frac{K_{UO_2}}{1 + K_{UO_2}(\Delta A(\mathrm{Er}) + \Delta B(\mathrm{Er})T)}. \tag{13}$$

Since $\Delta A(\mathrm{Er})$ and $\Delta B(\mathrm{Er})$ are proportional to the Er-atom content as shown in Figs. 4 and 5, Eq. (13) is expressed by

$$K = \frac{K_{UO_2}}{1 + K_{UO_2}(k_A y + k_B y T)}, \tag{14}$$

where k_A and k_B are the slopes in Figs. 4 and 5, respectively and y is the Er content in the $(U_{1-y}Er_y)O_2$ solid solution.

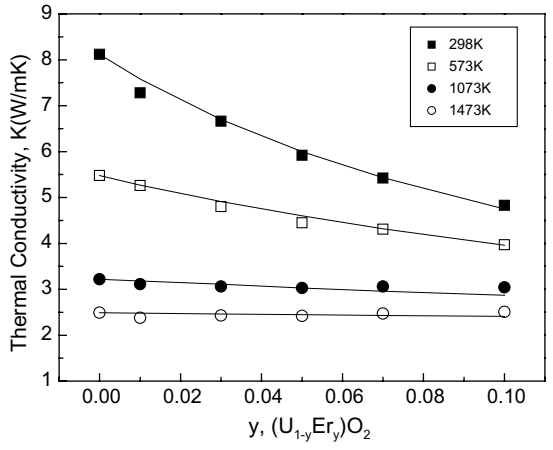

Fig. 6. Comparison of the experimental and calculated thermal conductivities of $(U,Er)O_2$. Symbols and solid lines are obtained from Eqs. (5) and (14), respectively.

Fig. 6 shows the thermal conductivities calculated from Eq. (14) and the experimental ones determined from Eq. (5) as a function of the $ErO_{1.5}$ content. The symbols and solid lines in Fig. 6 correspond to the experimental data and calculated values, respectively. As shown in Fig. 6, Eq. (14) is a good model of the thermal conductivity of near-stoichiometric $(U,Er)O_2$ solid solutions as a function of $ErO_{1.5}$ content, up to 10 mol %, in the temperature range between room temperature and 1673 K.

4. Summary

Thermal diffusivities of UO_2 and $(U,Er)O_2$ solid solutions were measured from room temperature to 1673 K by a laser flash method. Their thermal conductivities were calculated by multiplying the thermal diffusivities, the specific heat capacities and the sample densities. The thermal diffusivities and thermal conductivities of each sample decreased with increasing the temperature. The thermal conductivities decreased with an increasing $ErO_{1.5}$ at a low temperature, while at high temperatures they were independent of the $ErO_{1.5}$ content.

The thermal conductivities of $(U,Er)O_2$ can be expressed as a function of the $ErO_{1.5}$ content by the following equation, which is derived from the phonon conduction equation,

$$K = \frac{K_{UO_2}}{1 + K_{UO_2}(k_A y + k_B y T)}.$$

Acknowledgement

We acknowledge that this project has been carried out under the Nuclear R&D Program by the Ministry of Science and Technology.

References

[1] L. Goldstein, A.A. Strasser, Nucl. Technol. 60 (1983) 352.
[2] H.S. Kim, Y.K. Yoon, M.S. Yang, J. Nucl. Mater. 209 (1994) 286.
[3] H.S. Kim, Y.K. Yoon, Y.W. Lee, J. Nucl. Mater. 226 (1995) 206.
[4] S. Fukushima, T. Ohmichi, A. Maeda, H. Watanabe, J. Nucl. Mater. 105 (1982) 201.
[5] M. Hirai, S. Ishimoto, J. Nucl. Sci. Technol. 28 (1991) 995.
[6] T. Matsui, Y. Arita, K. Naito, J. Nucl. Mater. 188 (1992) 205.
[7] M. Amaya, M. Hirai, T. Kubo, Y. Korei, J. Nucl. Mater. 231 (1996) 29.
[8] M. Amaya, M. Hirai, J. Nucl. Mater. 246 (1997) 158.
[9] M. Amaya, M. Hirai, H. Sakurai, K. Ito, M. Sasaki, T. Nomata, K. Kamimura, R. Iwasaki, J. Nucl. Mater. 300 (2002) 57.
[10] J.H. Yang, K.S. Kim, K.W. Kang, S.W. Song, J.H. Kim, Proc. Kor. Nucl. Soc. Korea, May 2001.
[11] H.S. Kim, S.H. Kim, Y.W. Lee, S.H. Na, J. Kor. Nucl. Soc. 28 (1996) 458.
[12] K. Une, M. Oguma, J. Nucl. Mater. 110 (1985) 215.
[13] H. Tagawa, T. Fujino, J. At. Energ. Soc. Jpn. 22 (1980) 871.
[14] S. Fukushima, T. Ohmichi, A. Maeda, M. Handa, J. Nucl. Mater. 114 (1983) 312.
[15] S. Fukushima, T. Ohmichi, A. Maeda, H. Watanabe, J. Nucl. Mater. 102 (1981) 30.
[16] T. Ohmichi, S. Fukushima, A. Maeda, H. Watanabe, J. Nucl. Mater. 102 (1981) 401.
[17] R.D. Shannon, Acta Crystallogr. A 32 (1976) 751.
[18] R. Brandt, G. Neuer, J. Non-Equilib. Thermodyn. 1 (1976) 3.
[19] World Wide Web, INSC Materials Properties Database, http://www.insc.anl.gov/matprop/.
[20] Outokumpu HSC Chemistry for Windows Ver. 4.1 (software), 1999.
[21] P.G. Klemens, Proc. Phys. Soc. A 68 (1955) 1113.
[22] W.D. Kingery, J. Am. Ceram. Soc. 42 (1959) 617.